# Solvatochromism and Preferential Solvation of Brooker's Merocyanine in Water–Methanol Mixtures

Yuichi Tanaka [a], Yukio Kawashima [b], Norio Yoshida *[a] and Haruyuki Nakano *[a]

The excitation energy of Brooker's merocyanine in water–methanol mixtures shows nonlinear behavior with respect to the mole fraction of methanol, and it was suggested that this behavior is related to preferential solvation by methanol. We investigated the origin of this behavior and its relation to preferential solvation using the three-dimensional reference interaction site model self-consistent field method and time-dependent density functional theory. The calculated excitation energies were in good agreement with the experimental behavior. Analysis of the coordination numbers revealed preferential solvation by methanol. The free energy component analysis implied that solvent reorganization and solvation entropy drive the preferential solvation by methanol, while the direct solute–solvent interaction promotes solvation by water. The difference in the preferential solvation effect on the ground and excited states causes the nonlinear excitation energy shift. © 2017 Wiley Periodicals, Inc.

DOI: 10.1002/jcc.24902

## Introduction

Preferential solvation, a phenomenon whereby a solute is solvated more preferentially by one solvent than by others, usually occurs in a mixed solvent, and the local mole fractions of a solvent around the solute differ from the bulk mole fractions.[1] Preferential solvation has attracted the attention of researchers because many chemical reactions and biological processes occur in a mixed solvent, and the environment around a solute has a large influence on the reaction and physical properties.[2–6]

The solvatochromic shift of absorption and emission spectra is strongly affected by preferential solvation because the solvation structure near the solute molecules drastically changes the electronic structure of the solute molecules. A binary or multicomponent mixed solvent is useful to control the solvatochromic shift by changing the mole fraction of the components. 1-Methyl-4-[(oxocyclohexadienylidene)ethylidene]-1,4-dihydropyridine, which is often called Brooker's merocyanine (BM, Fig. 1), is a famous and typical solvatochromic dye that is used as a target to investigate the effects of preferential solvation on the solvatochromic shift because of its high responsiveness.[7]

Da Silva et al.[8] measured the absorption spectra of BM in binary mixtures comprising a protic solvent (water, methanol, ethanol, 2-propanol, or 1-butanol) and aprotic solvent (acetonitrile, dimethyl sulfoxide, or acetone) in various mole fractions. In water–methanol mixtures, they obtained a nonlinear excitation energy behavior with respect to the mole fraction and concluded that the origin for the nonlinearity was preferential solvation by methanol. Although the experimental observations suggested a phenomenological relation between the solvatochromic shift and the preferential solvation, the molecular-level understanding of this process is still insufficient.

Theoretical approaches are desirable to understand the detailed solvation structure at a molecular level. One effective theoretical approach is quantum mechanics/molecular mechanics (QM/MM),[9] which is widely used to investigate both the electronic structure of the solvated molecule and the solvation structure. In this method, the solvent environment is treated as an explicit molecule with a classical force field placed around the solute molecule based on the configuration sampling by molecular dynamics simulation. Frutos-Puerto et al.[10] investigated the solvatochromic shift of *p*-nitroaniline in cyclohexane–triethylamine mixtures using a mean-field QM/MM method.[11–13] The computed excitation energies were in good agreement with the experiments, showing the nonlinear behavior of the excitation energy with respect to the mole fraction. The solvent composition surrounding *p*-nitroaniline was significantly different from that of the bulk; this observation clearly indicates preferential solvation. Although the QM/MM method has been successfully applied to study the electronic structure of solvated molecules, QM/MM studies of mixed solvents are not common. One reason is that the QM/MM method requires extensive computational cost and time for configuration sampling of a multicomponent solvent, especially for dilute components, because the convergence of such sampling is generally very slow.

Another possible method for investigating solvatochromism in mixtures is a hybrid of the integral equation theory of liquids and electronic structure theory, such as reference interaction site model self-consistent field (RISM-SCF),[14–16] three-dimensional RISM-SCF (3D-RISM-SCF),[17] or Kohn–Sham density functional theory (KS-DFT)/3D-RISM methods.[18] These methods have

[a] Y. Tanaka, N. Yoshida, H. Nakano
Department of Chemistry, Graduate School of Science, Kyushu University, 744 Motooka, Nishi-ku, Fukuoka 819-0395, Japan
E-mail: noriwo@chem.kyushu-univ.jp, E-mail: nakano@chem.kyushu-univ.jp
[b] Y. Kawashima
RIKEN Advanced Institute for Computational Science, 7-1-26, Minatojima-minami-machi, Chuo-ku, Kobe, Hyogo 650-0047, Japan
Contract grant sponsor: JSPS KAKENHI; Contract grant numbers: 15J04698, 16K05676, 16K05519, and 15K05392; Contract grant sponsor: MEXT KAKENHI; Contract grant number: 16H00842

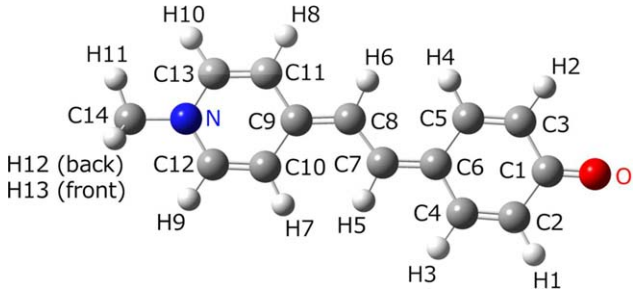


**Figure 1**. The molecular structure of Brooker's merocyanine. [Color figure can be viewed at wileyonlinelibrary.com]

been successfully applied to the solvatochromism of dyes in various single component solutions.[19–22] An advantage of the hybrid method is that it is easily applicable to multicomponent solutions because the integral equation theory of liquids allows one to obtain the solvation structure of multiple components from the complete ensemble average based on statistical mechanics. Pioneering work to investigate the electronic structure of molecules in a mixed solvent using the hybrid methods was done by Hayaki et al.[23]; they performed a theoretical analysis of a Diels–Alder reaction in ionic liquids. Following their work, many works have been devoted to chemical reactions in ionic liquids,[24–28] electrolyte solutions,[29–31] and water–organic mixed solvents.[32] For all these studies, the RISM/3D-RISM-SCF and extended hybrid methods gave reasonable results and reproduced the nature of the chemical reactions in mixed solvents.

In the present study, we investigated the solvatochromism of BM in water–methanol mixtures using the 3D-RISM-SCF method and TD-DFT to clarify the details of preferential solvation of BM (as suggested by Da Silva et al.[8]) at the molecular level. Although both water and methanol are protic solvents, their abilities to form hydrogen bonds are different because water has two hydroxyl hydrogen atoms while methanol has one hydroxyl hydrogen atom and one methyl group. We performed 3D-RISM-SCF calculations and obtained the excitation energy changes for BM as well as the spatial distribution of the solvent in various mole fractions of water–methanol mixtures. From the results, we examined the relation between the solute–solvent interactions and coordination numbers (CNs) to theoretically clarify the origin of the excitation energy behavior (i.e., preferential solvation or not). A free energy component analysis for the solvation structure was also performed to discuss the mechanism of preferential solvation.

## Computational Methods

### Brief overview of the 3D-RISM-SCF method

We performed 3D-RISM-SCF and TD-DFT calculations to obtain the vertical excitation energies of BM in water–methanol mixtures. The 3D-RISM-SCF method is a hybrid method of the electronic structure theory and integral equation theory of liquids (3D-RISM theory).[33,34] In this method, solute molecules are treated quantum-chemically and solvent molecules are treated statistical-mechanically; thereby, the electronic wave function of the solute and the distribution of the solvent (spatial distribution function [SDF], $g_\gamma(\mathbf{r})$; $\gamma$ indicates the solvent site) around the solute are determined simultaneously.

The Helmholtz free energy ($A$) of a system is defined as the sum of the solute electronic energy ($E_{\text{solute}}$) and the excess chemical potential ($\Delta\mu$):

$$A = E_{\text{solute}} + \Delta\mu. \tag{1}$$

$E_{\text{solute}}$ is calculated from an electronic structure calculation:

$$E_{\text{solute}} = < \Psi^{\text{solv}} | \hat{\text{H}}_0 | \Psi^{\text{solv}} >, \tag{2}$$

where $\hat{\text{H}}_0$ is the Hamiltonian of the isolated solute molecule and $\Psi^{\text{solv}}$ is the electronic wave function of the solute molecule in solution. $\Delta\mu$ is calculated from the following equation:

$$\Delta\mu = k_{\text{B}}T \sum_v \rho_v \sum_{\gamma\in v} \int d\mathbf{r} \left[ \frac{1}{2} \left( h_\gamma(\mathbf{r}) \right)^2 \Theta\left( -h_\gamma(\mathbf{r}) \right) - c_\gamma(\mathbf{r}) - \frac{1}{2} h_\gamma(\mathbf{r}) c_\gamma(\mathbf{r}) \right], \tag{3}$$

where $k_{\text{B}}$ and $T$ indicate the Boltzmann constant and the absolute temperature, respectively, and $\rho_v$ is the number density of solvent species $v$. The functions $h_\gamma(\mathbf{r}) = g_\gamma(\mathbf{r}) - 1$ and $c_\gamma(\mathbf{r})$ are the 3D total and direct correlation functions of solvent site $\gamma$, respectively, and $\Theta(x)$ is the Heaviside step function. To derive eq. (3), we applied the Kovalenko–Hirata (KH) closure[18]:

$$h_\gamma(\mathbf{r}) = \begin{cases} \exp\left( -u_\gamma(\mathbf{r})/k_{\text{B}}T + h_\gamma(\mathbf{r}) - c_\gamma(\mathbf{r}) \right) - 1 & \text{for } h_\gamma(\mathbf{r}) \le 0 \\ -u_\gamma(\mathbf{r})/k_{\text{B}}T + h_\gamma(\mathbf{r}) - c_\gamma(\mathbf{r}) & \text{for } h_\gamma(\mathbf{r}) > 0 \end{cases}, \tag{4}$$

where $u_\gamma(\mathbf{r})$ is the interaction potential between the solute molecule and solvent site $\gamma$. 3D correlation functions can be obtained by solving the 3D-RISM equation [eq. (5)] coupled with the KH closure [eq. (4)]:

$$h_\gamma(\mathbf{r}) = c_{\gamma'}(\mathbf{r}) * \left( \omega^{\text{vv}}_{\gamma'\gamma}(r) + \rho_v h^{\text{vv}}_{\gamma'\gamma}(r) \right), \tag{5}$$

where $\omega^{\text{vv}}_{\gamma\gamma'}(r)$ and $h^{\text{vv}}_{\gamma\gamma'}(r)$ are the site–site intramolecular and total correlation functions of the solvent, respectively (superscript "v" denotes the solvent). The symbol * indicates convolution in direct space and summation over repeated site indices. Before the 3D-RISM calculation, we need to solve the (1D) RISM equation between the solvent molecules [eq. (6)] and obtain $h^{\text{vv}}_{\gamma\gamma'}(r)$ in eq. (5):

$$h^{\text{vv}}_{\gamma\gamma'}(r) = \omega^{\text{vv}}_{\gamma\gamma''}(r) * c^{\text{vv}}_{\gamma''\gamma'''}(r) * \left( \omega^{\text{vv}}_{\gamma'''\gamma'}(r) + \rho_v h^{\text{vv}}_{\gamma'''\gamma'}(r) \right), \tag{6}$$

where $c^{\text{vv}}_{\gamma\gamma'}(r)$ indicates the site–site direct correlation function of the solvent molecules.

### Computational details

The molecular structure of BM was optimized in pure water (mole fraction of methanol ($X_{\text{m}}$) = 0.0), water–methanol mixtures ($X_{\text{m}}$ = 0.1–0.9 at intervals of 0.1), and pure methanol ($X_{\text{m}}$ = 1.0)

**Table 1.** The number densities of water ($\rho_w$) and methanol ($\rho_m$) in the solutions.

| $X_m$ | $\rho_w$ (molecules Å$^{-3}$) | $\rho_m$ (molecules Å$^{-3}$) |
|---|---|---|
| 0.0 | 0.033316 | 0.000000 |
| 0.1 | 0.026644 | 0.002960 |
| 0.2 | 0.021309 | 0.005327 |
| 0.3 | 0.016946 | 0.007263 |
| 0.4 | 0.013313 | 0.008875 |
| 0.5 | 0.010239 | 0.010239 |
| 0.6 | 0.007605 | 0.011407 |
| 0.7 | 0.005323 | 0.012420 |
| 0.8 | 0.003326 | 0.013306 |
| 0.9 | 0.001565 | 0.014087 |
| 1.0 | 0.000000 | 0.014781 |

using the 3D-RISM-SCF calculation. In the DFT and TD-DFT parts of the calculations, we used the long-range corrected Becke one-parameter progressive (LC-BOP) exchange-correlation functional[35] and the augmented correlation-consistent polarized valence double-zeta (aug-cc-pVDZ) basis set.[36,37] The long-range correction in the exchange functional is necessary for excitation energy calculations because the excitation of BM has some charge transfer character. Our previous study[22] confirmed the validity of the LC-BOP by comparing the solvent dependence of the excitation energy with the LC Becke Lee–Yang–Parr (LC-BLYP)[38] and Coulomb-attenuating method Becke three-parameter Lee–Yang–Parr (CAM-B3LYP)[39] functionals. The aug-cc-pVDZ was selected because the diffuse function expresses the negative charge on the phenoxide oxygen atom.

In the 3D-RISM part of the calculations, the sum of the Coulomb and Lennard-Jones (LJ) potentials,

$$u_\gamma(\mathbf{r}) = -\sum_i \int d\mathbf{r}' \frac{|\phi_i(\mathbf{r}')|^2 q_\gamma}{|\mathbf{r}-\mathbf{r}'|} + \sum_\alpha \frac{Z_\alpha q_\gamma}{|\mathbf{r}-\mathbf{r}_\alpha|} + \sum_\alpha 4\varepsilon_{\alpha\gamma}\left[\left(\frac{\sigma_{\alpha\gamma}}{|\mathbf{r}-\mathbf{r}_\alpha|}\right)^{12} - \left(\frac{\sigma_{\alpha\gamma}}{|\mathbf{r}-\mathbf{r}_\alpha|}\right)^{6}\right], \quad (7)$$

was chosen as $u_\gamma(\mathbf{r})$, where $\phi_i(\mathbf{r}')$ is a KS molecular orbital storing electron $i$, $Z_\alpha$ indicates the nuclear charge of solute site $\alpha$, and $q_\gamma$ denotes the partial charge of solvent site $\gamma$. The LJ parameters, $\sigma_{\alpha\gamma}$ and $\varepsilon_{\alpha\gamma}$, were obtained based on the Lorentz–Berthelot combining rule:

$$\sigma_{\alpha\gamma} = \frac{\sigma_\alpha + \sigma_\gamma}{2}, \quad (8)$$

$$\varepsilon_{\alpha\gamma} = \sqrt{\varepsilon_\alpha \varepsilon_\gamma}. \quad (9)$$

The optimized potentials for liquid simulations (OPLS) parameters were used for BM and methanol.[40,41] The parameters for water were taken from the extended simple point charge model (SPC/E).[42] The LJ parameters for the hydroxyl hydrogen atoms of the two solvents were $\sigma = 0.4$ Å and $\varepsilon = 0.046$ kcal mol$^{-1}$. The number densities of water and methanol in the solutions are summarized in Table 1. The densities were calculated using the densities of the pure solvents and molar masses of the solvent molecules; we did not consider the volume change caused by mixing. Here, we assumed that the effect of the volume change on the solvatochromic shift was small. To assess this assumption, we examined the excitation energy of BM using the experimental density[43] at $X_m = 0.3599$, where the difference between the ideal (0.8795 g cm$^{-3}$) and experimental (0.9119 g cm$^{-3}$) densities is the largest (0.0324 g cm$^{-3}$) at the measured mole fractions. The excitation energies of the two densities differed by only 0.017 eV; therefore, the following discussion is not affected. The temperature was set at 298.15 K. Rectangular grid boxes, the axes of which had 128 grid points with a spacing of 0.5 Å, were used in the 3D-RISM calculations.

All calculations were performed using a modified version[44] of the GAMESS program package.[45]

## Results and Discussion

### Excitation energy of BM in water–methanol mixtures

First, we briefly mention the lowest excited state of BM that is involved in solvatochromism. The main configuration of the lowest excited state is the highest occupied molecular orbital (HOMO)–lowest unoccupied molecular orbital (LUMO) configuration. The HOMO and LUMO of solvated BM (pure water [$X_m = 0.0$] and methanol [$X_m = 1.0$]) and isolated BM are shown in Figure 2. Both the HOMO and LUMO are $\pi$-type orbitals. As mentioned in our previous study,[22] both the HOMO and LUMO are delocalized over the entire molecule for isolated BM. However, the HOMO is mainly localized around the phenoxide moiety, whereas the LUMO is mainly localized around the pyridine moiety for solvated BM. Thus, the HOMO–LUMO excitation has some intramolecular charge transfer character in the water–methanol mixture, as mentioned in the Computational Methods. In addition, the localization of the HOMO and LUMO in pure water is larger than that in pure methanol.

In Figure 3, the calculated excitation energy (using the 3D-RISM-SCF method and TD-DFT) and the experimental excitation energy are plotted against $X_m$ for the water–methanol mixture (the function form and parameters for fitting the experimental values were taken from Ref. 8). The broken lines in the figure are straight lines that connect the values of pure water and pure methanol and show the interpolated values for the excitation energy. The calculated excitation energies in pure water and methanol are 3.42 eV and 2.91 eV, respectively; the value in water is larger than that in methanol, which is in qualitative agreement with the experiment [water: 2.81 eV, methanol: 2.57 eV (Ref. 7); water: 2.79 eV, methanol: 2.55 eV (Ref. 8)]. In addition, we observe common characteristics for the calculations and experiments: the excitation energy monotonically decreases with increasing $X_m$, and the excitation energy has a more concave curve than the straight line that connects the pure solvent values. The maximum difference between the calculated and interpolated values is 0.045 eV at $X_m = 0.5$, whereas that between the experimental and interpolated values is about 0.063 eV at approximately $X_m = 0.4$. These data indicate that the effect of methanol addition to pure water is larger than that expected from the linear

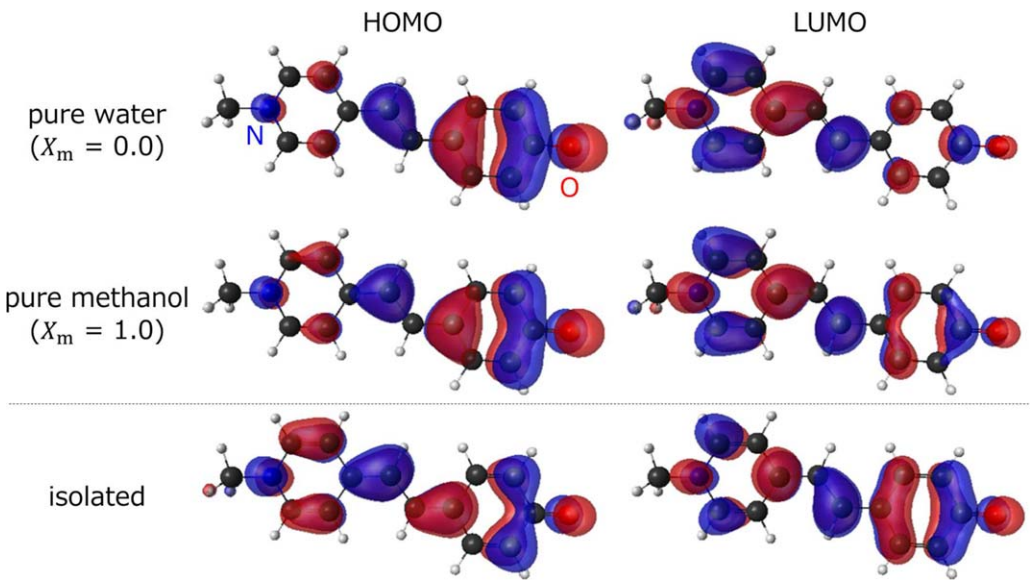


**Figure 2**. HOMO and LUMO of solvated Brooker's merocyanine (pure water [$X_m = 0.0$] and methanol [$X_m = 1.0$]) and isolated Brooker's merocyanine. The isovalues are 0.03. These orbitals were visualized using the MacMolPlt software.[46] [Color figure can be viewed at wileyonlinelibrary.com]

interpolation between pure water and pure methanol. From this behavior, Da Silva et al.[8] suggested that more methanol molecules are present around BM than would be expected from its mole fraction; that is, methanol preferentially solvates BM in this mixture. However, there has been no direct data showing preferential solvation by methanol.

We first consider the SDF given by the 3D-RISM-SCF calculation, which shows the solvent distribution around BM. Figure 4 shows the SDFs around BM in a mixture ($X_m = 0.5$). The hydroxyl hydrogen atoms of water and methanol both distribute near the O site (the phenoxide oxygen atom), and distributions of oxygen atoms are observed outside this region, indicating that the hydroxyl hydrogen atoms of the solvent form hydrogen bonds with the O site. The areas of hydroxyl hydrogen distribution for both solvents are almost the same, whereas the area of methanol oxygen distribution is much smaller than that of water oxygen distribution. Instead, the methyl group of methanol is more distributed around the hydrophobic surface of BM and less distributed around the hydrophilic groups.

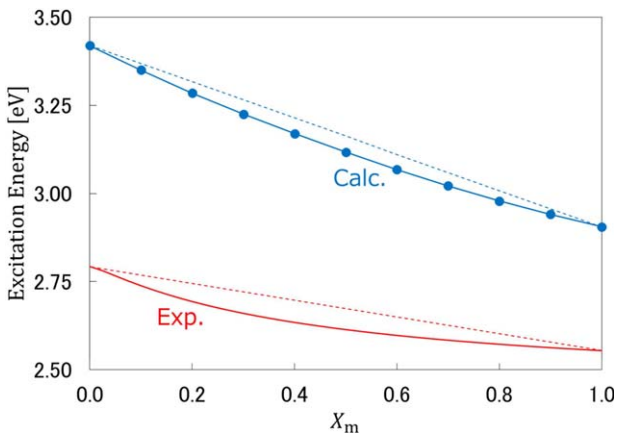


**Figure 3**. The excitation energies of Brooker's merocyanine with respect to the mole fraction of methanol, $X_m$. The experimental curve is described using the function and parameters taken from Ref. [8]. [Color figure can be viewed at wileyonlinelibrary.com]

Although the SDF (a direct output of the 3D-RISM-SCF calculation) shows the solvent surrounding the solute in detail, it is not very suitable to quantify the difference in the distribution magnitude between the two solvents. Therefore, in the following, we discuss the solvent distribution using the CNs of the solvent around specific BM sites. First, to determine the most important site of the BM, that is, the target to investigate the CNs, we analyzed the solute–solvent binding energy. The total of the solute–solvent binding energies between BM and two solvents ($E_{BM}^{bind,PC}$) and the solute–solvent binding energy between BM and solvent species $v$ ($E_{BMv}^{bind,PC}$) are calculated from the following equations:

$$E_{BM}^{bind,PC} = \sum_v E_{BMv}^{bind,PC}, \tag{10}$$

$$E_{BMv}^{bind,PC} = \rho_v \sum_\alpha \sum_{\gamma \in v} \int d\mathbf{r} g_\gamma(\mathbf{r}) u_{\alpha\gamma}^{PC}(\mathbf{r}), \tag{11}$$

$$u_{\alpha\gamma}^{PC}(\mathbf{r}) = \frac{q_\alpha q_\gamma}{|\mathbf{r}-\mathbf{r}_\alpha|} + 4\varepsilon_{\alpha\gamma}\left[\left(\frac{\sigma_{\alpha\gamma}}{|\mathbf{r}-\mathbf{r}_\alpha|}\right)^{12} - \left(\frac{\sigma_{\alpha\gamma}}{|\mathbf{r}-\mathbf{r}_\alpha|}\right)^{6}\right], \tag{12}$$

where $q_\alpha$ indicates the partial charge of solute site $\alpha$ and is calculated by least squares fitting, and the superscript "PC" indicates the quantities evaluated using the partial charge approximation for the solute molecule. In this approximation, the electrostatic interaction between the solute and solvent molecules is expressed as the sum of the Coulomb interaction between the partial charge on the solute and solvent sites. By this treatment, the binding energy can be decomposed into the contributions at each solute site. Here, the *binding energy* is defined as negative for bound states for convenience. Figure 5 shows $E_{BM}^{bind,PC}$ and $E_{BMv}^{bind,PC}$ with respect to $X_m$. The binding energy attributed to methanol ($E_{BMm}^{bind,PC}$) is lower than the linear

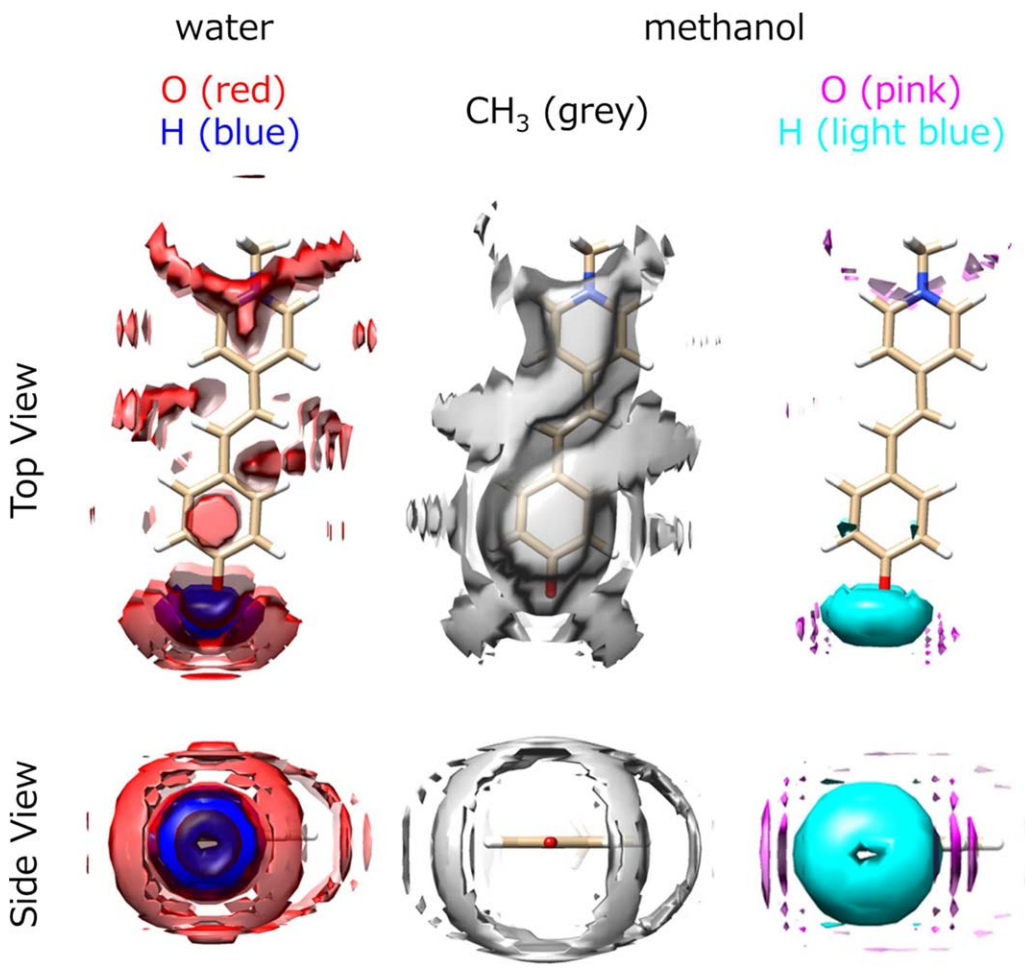


**Figure 4.** Isosurface plots of the SDFs around Brooker's merocyanine in a water–methanol mixture ($X_m = 0.5$) (water: O [isovalue = 2.5], H [isovalue = 2.0]; methanol: $CH_3$ [isovalue = 2.5], O [isovalue = 2.5], H [isovalue = 2.0]). These SDFs were visualized using the UCSF Chimera software.[48] [Color figure can be viewed at wileyonlinelibrary.com]

interpolation value, whereas that attributed to water ($E_{BMw}^{bind,PC}$) is higher than the linear interpolation value. The largest differences between the calculated and interpolated binding energies are 19.84 kcal mol$^{-1}$ (water) and −14.58 kcal mol$^{-1}$ (methanol), and both are observed at $X_m = 0.5$. In addition,

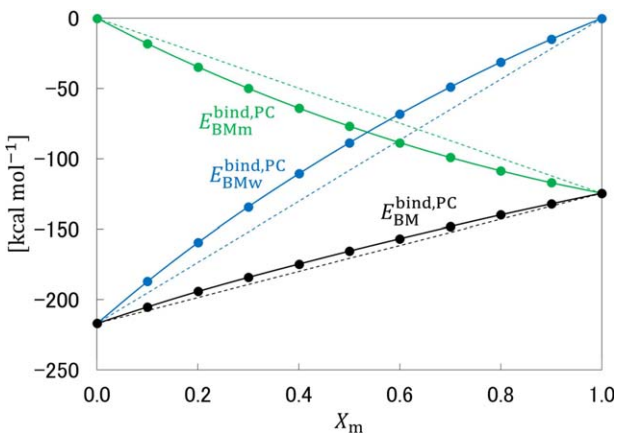


**Figure 5.** The solute–solvent binding energies between Brooker's merocyanine and the solvents ($E_{BM}^{bind,PC}$, $E_{BMw}^{bind,PC}$, and $E_{BMm}^{bind,PC}$) with respect to $X_m$. [Color figure can be viewed at wileyonlinelibrary.com]

$E_{BM}^{bind,PC}$ is higher than the linear interpolation value. These results suggest the existence of preferential solvation.

Table 2 shows the total of the solute–solvent binding energies between solute site $\alpha$ and two solvents ($E_{\alpha}^{bind,PC}$), and the solute–solvent binding energy between solute site $\alpha$ and solvent species $\nu$ ($E_{\alpha\nu}^{bind,PC}$) for $X_m = 0.5$:

$$E_{\alpha}^{bind,PC} = \sum_{\nu} E_{\alpha\nu}^{bind,PC}, \tag{13}$$

$$E_{\alpha\nu}^{bind,PC} = \rho_{\nu} \sum_{\gamma \in \nu} \int d\mathbf{r} g_{\gamma}(\mathbf{r}) u_{\alpha\gamma}^{PC}(\mathbf{r}). \tag{14}$$

The labels for each site are shown in Figure 1. The difference between the binding energy for $X_m = 0.5$ and that of the linear interpolation value is also shown in the table. The binding energy at the O site ($E_{O}^{bind,PC}$) is overwhelmingly larger than that at the other sites. The binding energies between the O site and water ($E_{Ow}^{bind,PC}$) and methanol ($E_{Om}^{bind,PC}$) are −84.51 kcal mol$^{-1}$ and −58.45 kcal mol$^{-1}$, respectively, which are more than twice that of the other values. The values at the O site also show the largest deviation from the interpolated values. The same trend is observed at other mole fractions.

**Table 2.** The solute–solvent binding energies at all Brooker's merocyanine sites for $X_m = 0.5$.[a]

| Site | Water (kcal mol$^{-1}$) | Methanol (kcal mol$^{-1}$) | Total (kcal mol$^{-1}$) |
|---|---|---|---|
| O | −84.51 (17.24) | −58.45 (−8.92) | −142.96 (8.32) |
| C1 | 40.06 (−1.91) | 27.14 (0.74) | 67.20 (−1.17) |
| C2 | −15.21 (0.81) | −11.60 (−0.69) | −26.81 (0.13) |
| H1 | 5.18 (−0.66) | 3.64 (0.26) | 8.82 (−0.40) |
| C3 | −16.26 (0.31) | −12.30 (−0.60) | −28.56 (−0.30) |
| H2 | 5.43 (−0.44) | 3.79 (0.25) | 9.21 (−0.20) |
| C4 | −3.07 (0.78) | −2.90 (−0.31) | −5.97 (0.47) |
| H3 | 1.58 (−0.26) | 0.98 (0.04) | 2.56 (−0.22) |
| C5 | −2.02 (0.76) | −2.12 (−0.50) | −4.14 (0.26) |
| H4 | 1.57 (−0.16) | 0.94 (0.01) | 2.51 (−0.15) |
| C6 | −0.75 (−0.20) | −1.25 (−0.26) | −1.99 (−0.46) |
| C7 | −0.45 (0.22) | −1.00 (−0.26) | −1.45 (−0.04) |
| H5 | −0.35 (0.02) | −0.53 (−0.13) | −0.87 (−0.11) |
| C8 | 0.86 (0.18) | 0.25 (−0.03) | 1.12 (0.15) |
| H6 | −0.66 (0.07) | −0.78 (−0.18) | −1.44 (−0.10) |
| C9 | −4.45 (0.42) | −4.36 (−0.50) | −8.81 (−0.07) |
| C10 | 3.76 (0.03) | 2.37 (−0.06) | 6.13 (−0.02) |
| H7 | −3.00 (0.18) | −2.59 (−0.27) | −5.59 (−0.09) |
| C11 | 3.69 (0.19) | 2.30 (−0.21) | 5.99 (−0.02) |
| H8 | −3.02 (0.13) | −2.61 (−0.24) | −5.63 (−0.11) |
| C12 | 1.12 (0.50) | 0.19 (−0.62) | 1.31 (−0.12) |
| H9 | −4.34 (0.13) | −3.66 (−0.19) | −8.00 (−0.07) |
| C13 | 1.55 (0.44) | 0.53 (−0.51) | 2.08 (−0.07) |
| H10 | −4.66 (0.16) | −3.93 (−0.24) | −8.60 (−0.08) |
| N | −6.93 (0.38) | −6.48 (−0.39) | −13.41 (−0.01) |
| C14 | 8.09 (0.25) | 5.64 (−0.07) | 13.72 (0.18) |
| H11 | −4.05 (0.09) | −3.45 (−0.23) | −7.49 (−0.14) |
| H12 | −3.88 (0.09) | −3.30 (−0.24) | −7.18 (−0.15) |
| H13 | −3.88 (0.09) | −3.30 (−0.24) | −7.18 (−0.15) |
| total | −88.60 (19.84) | −76.83 (−14.58) | −165.44 (5.26) |

[a] Numbers in parentheses indicate the difference from the interpolated binding energies.

Because the contribution of the O site to the binding energy is the largest, we investigated $E_O^{bind,PC}$ more closely. Figure 6 shows $E_O^{bind,PC}$, $E_{Ow}^{bind,PC}$, and $E_{Om}^{bind,PC}$ with respect to $X_m$. As with Figure 5, $E_{Om}^{bind,PC}$ is lower than the linear interpolation value and $E_{Ow}^{bind,PC}$ is higher than the linear interpolation value. The largest differences between the calculated and interpolated binding energies are 17.24 kcal mol$^{-1}$ (water) and −8.92 kcal mol$^{-1}$ (methanol) (both are observed at $X_m = 0.5$). In addition, $E_O^{bind,PC}$ is higher than the linear interpolation value, which is similar to $E^{bind,PC}$. These results suggest that preferential solvation occurs around the O site.

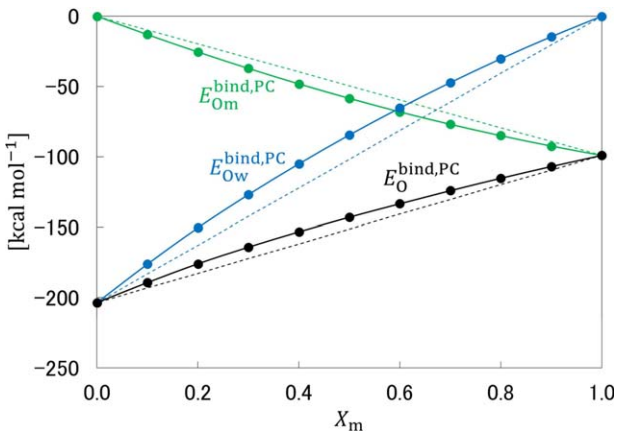


**Figure 6.** The solute–solvent binding energies between the O site of Brooker's merocyanine and the solvents ($E_O^{bind,PC}$, $E_{Ow}^{bind,PC}$, and $E_{Om}^{bind,PC}$) with respect to $X_m$. [Color figure can be viewed at wileyonlinelibrary.com]

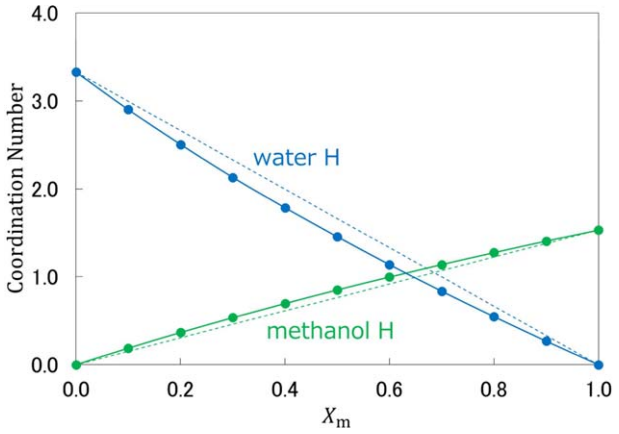


**Figure 7.** The CNs of the hydroxyl hydrogen atom in the first solvation shell around the O site with respect to $X_m$. [Color figure can be viewed at wileyonlinelibrary.com]

Figure 7 shows the CNs of the hydroxyl hydrogen atom in the first solvation shell around the O site. We examined the CNs of the hydroxyl hydrogen atom because the O site and the hydroxyl hydrogen atoms form hydrogen bonds (see Fig. 4). The CNs were obtained by radial integration of the radial distribution functions (RDFs) from the center to the first minimum of the RDFs (the RDFs were evaluated by angular-averaging of the SDFs over the solid angle around a specified center). The coordination of the hydroxyl hydrogen atom of methanol is larger and that of water is smaller than the linear interpolation value for all the mixtures ($X_m = 0.1$–$0.9$). These data directly show that preferential solvation occurs around the O site.

### Free energy component analysis

The analysis so far revealed that methanol has a larger CN than that from linear interpolation of the pure solvents for the site with the largest solute–solvent interaction. Such a solvation structure is not determined only from direct solute–solvent interactions; rather, it is determined by minimizing the free energy, including the solvent reorganization energy and solvation entropy, of the whole system. Therefore, free energy analysis is required to further understand the mechanism of preferential solvation.

The Helmholtz free energy ($A$) [eq. (1)] can be decomposed into components: the isolated solute electronic energy ($E_0$), the solute–solvent interaction energy ($E_{uv}$), the solvent reorganization energy ($E_{vv}$), and the solvation entropy multiplied by the absolute temperature ($-T\Delta S_v$)[29,48–50]:

$$\begin{aligned} A &= E_0 + E_{reorg} + \Delta\mu \\ &= E_0 + \Delta G_{solv} \\ &= E_0 + E_{uv} + E_{vv} - T\Delta S_v \end{aligned}, \quad (15)$$

$$E_{reorg} = E_{solute} - E_0, \quad (16)$$

$$\Delta G_{solv} = E_{reorg} + \Delta\mu = E_{uv} + E_{vv} - T\Delta S_v, \quad (17)$$

where $E_{reorg}$ and $\Delta G_{solv}$ are the electronic reorganization energy and the solvation free energy, respectively. $E_0$, $E_{uv}$, $E_{vv}$, and $\Delta S_v$ are calculated from the following equations:

$$E_0 = < \Psi_0^{solv} | \hat{H}_0 | \Psi_0^{solv} >, \quad (18)$$

$$E_{uv} = E_{reorg} + E^{bind} = E_{reorg} + \sum_v \rho_v \sum_{\gamma \in v} \int d\mathbf{r}\ g_\gamma(\mathbf{r}) u_\gamma(\mathbf{r}), \quad (19)$$

$$E_{vv} = 2\pi \sum_v \rho_v^2 \sum_{\gamma\gamma' \in v} \int dr\ r^2 \delta g_{\gamma\gamma'}^{vv}(r) u_{\gamma\gamma'}^{vv}(r), \quad (20)$$

$$\Delta S_v = -\left(\frac{\partial \Delta G_{solv}}{\partial T}\right)_{\rho_v}, \quad (21)$$

where $\Psi_0^{solv}$ is the electronic wave function of the isolated solute molecule, which maintains the optimized molecular structure in solution. The solute–solvent binding energy ($E^{bind}$) in eq. (19) is different from $E_{BM}^{bind,PC}$ in eq. (10). The difference is the solute–solvent interaction potential (in the case of $E^{bind}$, $u_\gamma(\mathbf{r})$ [eq. (7)] is used, whereas in the case of $E_{BM}^{bind,PC}$, $u_{\alpha\gamma}^{PC}(\mathbf{r})$ [eq. (12)] is used). The differences between $E^{bind}$ and $E_{BM}^{bind,PC}$ are 12.88 kcal mol$^{-1}$ ($X_m = 0.0$) and 5.45 kcal mol$^{-1}$ ($X_m = 1.0$). However, these differences do not affect the discussion. $\delta g_{\gamma\gamma'}^{vv}(r)$ is the first-order perturbation to $g_{\gamma\gamma'}^{vv}(r)$ (the RDF between solvent sites) by inserting the solute molecule at infinite dilution. $u_{\gamma\gamma'}^{vv}(r)$ is the interaction potential between the solvent sites. $E_{vv}$ indicates the energy arising from the structural changes induced in solution and has been calculated from the decomposition:

$$E_{vv} = \Delta G_{solv} - (E_{uv} - T\Delta S_v), \quad (22)$$

instead of eq. (20). The temperature derivative of the solvation free energy in eq. (21) is calculated using the first-order finite difference with $\Delta T = 1$ K. The solute molecular structures at 298.15 K were used in the 3D-RISM-SCF calculations at 298.15 ± 1 K.

Figure 8 shows the Helmholtz free energy and the components plotted as a function of $X_m$, where all the quantities are relative to the values at $X_m = 0$.

The relative Helmholtz free energy is negative and decreases with increasing $X_m$. This suggests that BM is more stable in solutions with higher values of $X_m$. The relative values of components $E_0$, $E_{vv}$, and $-T\Delta S_v$ are negative and decrease with increasing $X_m$, whereas the relative value of $E_{uv}$ is positive and increases with increasing $X_m$.

First, the decrease in $E_0$ is due to the reduction of solute–solvent electrostatic interactions. $E_0$ is higher for larger structural changes from the most stable molecular structure of isolated BM because it is the electronic energy of an isolated solute molecule (whose structure is optimized in solution). As $X_m$ increases, the solvent polarity decreases, which reduces the solute–solvent electrostatic interactions. The small solute–solvent electrostatic interaction provides a small structural change (for example, the differences of the O—C1 bond length between solvated and isolated BM are 0.098 Å (pure water [$X_m = 0.0$]) and 0.052 Å (pure methanol [$X_m = 1.0$]); thus, $E_0$ decreases. Next, the decrease in $E_{vv}$ is probably due to the reduced hydrogen bond network of the water molecules. $E_{vv}$ is the energy required for the solvent molecules to reorganize around a solute molecule by solvation. As $X_m$ increases, the hydrogen bond network of the water molecules decreases, and the solvent–solvent interactions decrease. Thus, $E_{vv}$ decreases. Similarly, the decreased number of hydrogen bonds reduces the value of $-T\Delta S_v$. Finally, $E_{uv}$ is the sum of the electronic reorganization energy ($E_{reorg}$) and the solute–solvent binding energy ($E^{bind}$). $E_{reorg}$ originates from the distortion of the electronic structure of BM because of immersion into the solvent. As $X_m$ increases, the solvent polarity decreases, and $E_{reorg}$ decreases. However, $E^{bind}$ increases with increasing $X_m$ (the case of $E_{BM}^{bind,PC}$ is shown in Fig. 5). The increase of $E^{bind}$ is larger than the decrease of $E_{reorg}$; therefore, $E_{uv}$ increases.

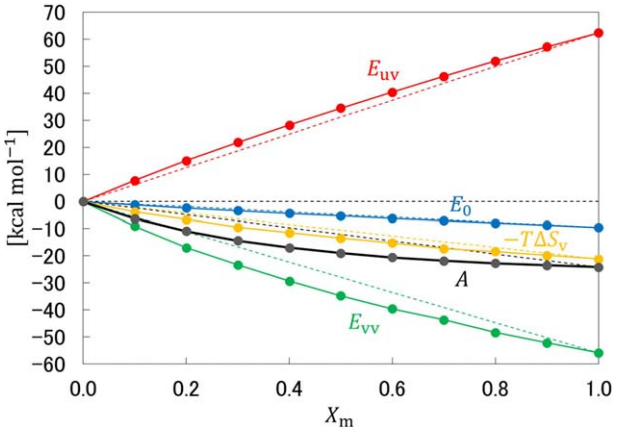


**Figure 8.** The Helmholtz free energy ($A$) and its components (the solute electronic energy [$E_0$], solute–solvent interaction energy [$E_{uv}$], solvent reorganization energy [$E_{vv}$], and solvation entropy [$-T\Delta S_v$]) with respect to $X_m$. [Color figure can be viewed at wileyonlinelibrary.com]

From Figure 8, we can also see that the Helmholtz free energy and its components, except for $E_{uv}$, have more concave curves than the interpolated line that connects the pure solvent values; $E_{uv}$ has a more convex curve. Thus, the Helmholtz free energy and its components show that the effect of methanol is larger than that expected from linear interpolation. The largest difference for $A$ from the interpolated value is −7.34 kcal mol$^{-1}$ at $X_m = 0.4$. The differences of the component values in the $X_m = 0.4$ mixture are −0.55 kcal mol$^{-1}$ ($E_0$), 3.26 kcal mol$^{-1}$ ($E_{uv}$), −7.01 kcal mol$^{-1}$ ($E_{vv}$), and −3.04 kcal mol$^{-1}$ ($-T\Delta S_v$). The solvent reorganization energy shows the largest deviation from the linear interpolation value. These results are common for all mixtures ($X_m = 0.1$–$0.9$).

The mechanism for preferential solvation by methanol to BM, implied by the above results, is as follows. Compared to water solvation to BM, methanol solvation destabilizes the solute–solvent interaction energy ($E_{uv}$) because the interaction of methanol with BM is weaker than that of water with BM. However, methanol solvation stabilizes the solvent reorganization energy

($E_{vv}$) and solvation entropy ($-T\Delta S_v$) because the reorganization of the methanol-rich solvent has a weaker hydrogen bond network than that of the water-rich solvent. The latter effect is dominant; thus, methanol preferentially binds to BM.

### Preferential solvation effect on the ground and excited states

Finally, to understand how the concave curves of the excitation energy in Figure 3 are formed, we separately examined the energy change of the ground and excited states. Figure 9 shows the energies of the ground and excited states plotted against $X_m$. The electronic energies of the ground and excited states become more destabilized as $X_m$ increases, which is due to the polarity decrease of the solvent. The dipole moment of the ground state is larger than that of the excited state; accordingly, the destabilization of the ground state is larger than that of the excited state. Both energies show convex curves compared to the linear interpolation lines. The difference from the interpolated energies in the ground state is larger than that in the excited state for the $X_m = 0.1$–$0.9$ mixtures; for example, the maximum differences are 5.02 eV (ground state at $X_m = 0.4$) and 4.97 eV (excited state at $X_m = 0.4$).

The concave behavior of the excitation energy is explained by the following consideration. Figure 10 shows a schematic representation of the energy dependence of the ground and excited states on $X_m$ and solvent polarity, where the gradients are emphasized more than the actual ones. The ground state has a zwitterionic nature; thus, its energy largely depends on the solvent polarity and decreases with increasing polarity. Conversely, the excited state has a weak ionic (almost neutral) nature; thus, its energy weakly depends on the polarity. The relationship between $X_m$ and solvent polarity is reversed (see Fig. 10) because methanol has a lower dielectric constant than water.

The solvent polarities at points A, B, and C (Fig. 10) shift from the expected values for the mole fractions to A′, B′, and C′, respectively, because of the preferential solvation by methanol. The solvent polarity shifts increase the energies of the ground and excited states from the values expected from the mole fraction, forming the convex energy curves in Figure 9. In addition, the gradient of the ground state is larger than that of the excited states; thus, we can easily understand that the upward energy shift of the ground state is larger than that of the excited state, providing the concave excitation energy curves in Figure 3.

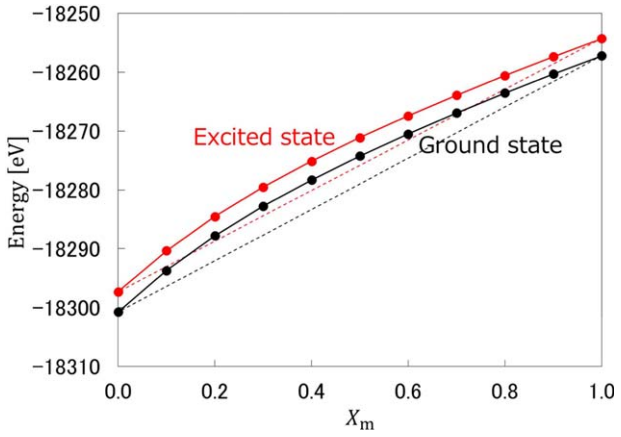


**Figure 9.** The energies of the ground and excited states with respect to $X_m$. [Color figure can be viewed at wileyonlinelibrary.com]

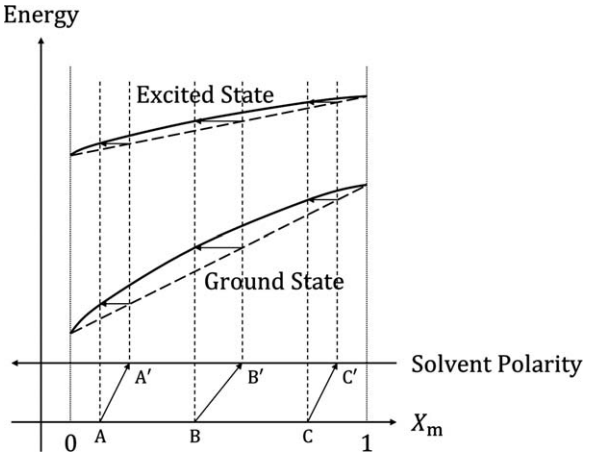


**Figure 10.** Schematic representation of the energy dependence of the ground and excited states on $X_m$ and solvent polarity.

## Conclusions

Preferential solvation around BM in water–methanol mixtures was investigated by calculating the solvatochromism using the 3D-RISM-SCF method. The excitation energies calculated using TD-DFT reproduced the nonlinear behavior (monotonic and concave decreases) with increasing values of $X_m$ in the experiments. The solvation structures obtained from the 3D-RISM calculations show that the phenoxide oxygen atom and the hydroxyl hydrogen atom of the solvent form hydrogen bonds, and the CNs show that methanol molecules solvate BM more preferentially than water molecules.

From the free energy component analysis, the Helmholtz free energy and its components also show nonlinear behaviors against $X_m$; these are caused by the preferential solvation by methanol. As $X_m$ increases, the solute–solvent interaction energy increases, whereas the solvent reorganization energy and solvation entropy decrease. These results may reflect the difference in the interaction between BM and water, BM and methanol, and water and methanol, such as hydrogen bonds. The trade-off between the components produces the preferential solvation by methanol.

The energies of the ground and excited states destabilize with increasing values of $X_m$ and show convex curves. The upward energy shift from the interpolated line is caused by solvent polarity, which is less than that based on $X_m$, and the shift of the ground state is larger than that of the excited state because the destabilization of the ground state is larger than that of the excited state. The excitation energy shows nonlinear concave behavior because of these shifts.

In this study, we assumed the homogeneity of the solvent environment; that is, $h^{vv}_{\gamma\gamma'}(r)$ obtained by solving the solvent–solvent RISM equation did not change during the solute–solvent 3D-RISM calculation, which is a standard treatment of the solvent in the integral equation theory of liquids. In other words, we assumed that the solvent–solvent correlation functions did not change because of the existence of BM. As demonstrated in this study, this assumption is valid for considering the effects of preferential solvation by methanol on the solvatochromic shift; however, the changes of the solvent–solvent correlation functions based on the inhomogeneity by the presence of the solute could affect the computed solvation structures when strong preferential solvation occurs. Therefore, an extended theory for inhomogeneous environments, such as inhomogeneous RISM theory,[51] should be used to describe the preferential solvation more universally. Such a study is in progress.

**Keywords:** solvatochromism · preferential solvation · Brooker's merocyanine · 3D-RISM-SCF method

How to cite this article: Y. Tanaka, Y. Kawashima, N. Yoshida, H. Nakano. *J. Comput. Chem*. **2017**, *38*, 2411–2419. DOI: 10.1002/jcc.24902

[1] C. Reichardt, T. Welton, Solvents and Solvent Effects in Organic Chemistry, 4th ed.; Wiley-VCH: Weinheim, **2011**.
[2] R. M. Tarkka, E. Buncel, *J. Am. Chem. Soc.* **1995**, *117*, 1503.
[3] C. Cativiela, J. I. García, J. Gil, R. M. Martínez, J. A. Mayoral, L. Salvatella, J. S. Urieta, A. M. Mainar, M. H. Abraham, *J. Chem. Soc. Perkin Trans.* **1997**, *2*, 653.
[4] A. Alimadadian, C. P. Colver, *Can. J. Chem. Eng.* **1976**, *54*, 208.
[5] K. Noda, M. Ohashi, K. Ishida, *J. Chem. Eng. Data* **1982**, *27*, 326.
[6] I.-C. Wei, R. L. Rowley, *J. Chem. Eng. Data* **1984**, *29*, 332.
[7] P. Jacques, *J. Phys. Chem.* **1986**, *90*, 5535.
[8] D. C. Da Silva, I. Ricken, M. A. D. R. Silva, V. G. Machado, *J. Phys. Org. Chem.* **2002**, *15*, 420.
[9] J. Gao, In Reviews in Computational Chemistry, Vol. *7*; K. B. Lipkowitz, D. B. Boyd, Eds.; Wiley-VCH: New York, **1996**; pp. 119–185.
[10] S. Frutos-Puerto, M. A. Aguilar, I. Fdez. Galván, *J. Phys. Chem. B* **2013**, *117*, 2466.
[11] M. L. Sánchez, M. A. Aguilar, F. J. Olivares del Valle, *J. Comput. Chem.* **1997**, *18*, 313.
[12] I. Fdez Galván, M. L. Sánchez, M. E. Martín, F. J. Olivares del Valle, M. A. Aguilar, *Comput. Phys. Commun.* **2003**, *155*, 244.
[13] M. A. Aguilar, M. L. Sánchez, M. E. Martín, I. F. Galván, In Continuum Solvation Models in Chemical Physics, 1st ed.; B. Mennucci, R. Cammi, Eds.; Wiley: New York, **2007**; Chapter 4.5, pp. 580–592.
[14] S. Ten-no, F. Hirata, S. Kato, *Chem. Phys. Lett.* **1993**, *214*, 391.
[15] S. Ten-no, F. Hirata, S. Kato, *J. Chem. Phys.* **1994**, *100*, 7443.
[16] H. Sato, F. Hirata, S. Kato, *J. Chem. Phys.* **1996**, *105*, 1546.
[17] H. Sato, A. Kovalenko, F. Hirata, *J. Chem. Phys.* **2000**, *112*, 9463.
[18] A. Kovalenko, F. Hirata, *J. Chem. Phys.* **1999**, *110*, 10095.
[19] Y. Tanaka, N. Yoshida, H. Nakano, *Chem. Phys. Lett.* **2013**, *583*, 69.
[20] K. Nishiyama, Y. Watanabe, N. Yoshida, F. Hirata, *J. Chem. Phys.* **2013**, *139*, 094503.
[21] T. Wada, H. Nakano, H. Sato, *J. Chem. Theory Comput.* **2014**, *10*, 4535.
[22] Y. Tanaka, N. Yoshida, H. Nakano, *J. Comput. Chem.* **2015**, *36*, 1655.
[23] S. Hayaki, K. Kido, D. Yokogawa, H. Sato, S. Sakaki, *J. Phys. Chem. B* **2009**, *113*, 8227.
[24] C. Chiappe, M. Malvaldi, C. S. Pomelli, *J. Chem. Theory Comput.* **2010**, *6*, 179.
[25] S. Hayaki, K. Kido, H. Sato, S. Sakaki, *Phys. Chem. Chem. Phys.* **2010**, *12*, 1822.
[26] S. Hayaki, Y. Kimura, H. Sato, *J. Phys. Chem. B* **2013**, *117*, 6759.
[27] Y. Nishimura, D. Yokogawa, S. Irle, *Chem. Phys. Lett.* **2014**, *603*, 7.
[28] Arifin, M. Puripat, D. Yokogawa, V. Parasuk, S. Irle, *J. Comput. Chem.* **2016**, *37*, 327.
[29] N. Yoshida, H. Tanaka, F. Hirata, *J. Phys. Chem. B* **2013**, *117*, 14115.
[30] Y. Kasai, N. Yoshida, H. Nakano, *J. Mol. Liq.* **2014**, *200*, 32.
[31] K. Kasahara, H. Nakano, H. Sato, *J. Phys. Chem. B* **2017**, *121*, 5293.
[32] Y. Kasai, N. Yoshida, H. Nakano, *J. Chem. Phys.* **2015**, *142*, 204103.
[33] D. Beglov, B. Roux, *J. Phys. Chem. B* **1997**, *101*, 7821.
[34] A. Kovalenko, F. Hirata, *Chem. Phys. Lett.* **1998**, *290*, 237.
[35] H. Iikura, T. Tsuneda, T. Yanai, K. Hirao, K. *J. Chem. Phys.* **2001**, *115*, 3540.
[36] T. H. Dunning, Jr., *J. Chem. Phys.* **1989**, *90*, 1007.
[37] R. A. Kendall, T. H. Dunning, Jr, R. J. Harrison, *J. Chem. Phys.* **1992**, *96*, 6796.
[38] Y. Tawada, T. Tsuneda, S. Yanagisawa, T. Yanai, K. Hirao, *J. Chem. Phys.* **2004**, *120*, 8425.
[39] T. Yanai, D. P. Tew, N. C. Handy, *Chem. Phys. Lett.* **2004**, *393*, 51.
[40] W. L. Jorgensen, D. S. Maxwell, J. Tirado-Rives, *J. Am Chem. Soc.* **1996**, *118*, 11225.
[41] W. L. Jorgensen, J. M. Briggs, M. L. Contreras, *J. Phys. Chem.* **1990**, *94*, 1683.
[42] H. J. C. Berendsen, J. R. Grigera, T. P. Straatsma, *J. Phys. Chem.* **1987**, *91*, 6269.
[43] S. Z. Mikhail, W. R. Kimel, *J. Chem. Eng. Data* **1961**, *6*, 533.
[44] N. Yoshida, F. Hirata, *J. Comput. Chem.* **2006**, *27*, 453.
[45] M. W. Schmidt, K. K. Baldridge, J. A. Boatz, S. T. Elbert, M. S. Gordon, J. H. Jensen, S. Koseki, N. Matsunaga, K. A. Nguyen, S. Su, T. L. Windus, M. Dupuis, J. A. Montgomery, Jr., *J. Comput. Chem.* **1993**, *14*, 1347.
[46] B. M. Bode, M. S. Gordon, *J. Mol. Graph. Model.* **1998**, *16*, 133.
[47] E. F. Pettersen, T. D. Goddard, C. C. Huang, G. S. Couch, D. M. Greenblatt, E. C. Meng, T. E. Ferrin, *J. Comput. Chem.* **2004**, *25*, 1605.
[48] H.-A. Yu, M. Karplus, *J. Chem. Phys.* **1988**, *89*, 2366.
[49] H.-A. Yu, B. Roux, M. Karplus, *J. Chem. Phys.* **1990**, *92*, 5020.
[50] T. Imai, Y. Harano, M. Kinoshita, A. Kovalenko, F. Hirata, *J. Chem. Phys.* **2006**, *125*, 204911.
[51] R. Ishizuka, S.-H. Chong, F. Hirata, *J. Chem. Phys.* **2008**, *128*, 034504.

Received: 17 May 2017
Revised: 29 June 2017
Accepted: 13 July 2017
Published online on 31 July 2017